ADVANCED FUNCTIONAL MATERIALS
www.afm-journal.de

Control the Entire Journey of Pesticide Application on Superhydrophobic Plant Surface by Dynamic Covalent Trimeric Surfactant Coacervation

Bin Liu, Yaxun Fan, Haofei Li, Weiwei Zhao, Siqi Luo, Hua Wang, Bo Guan, Qiaolian Li, Jiling Yue, Zhichao Dong,* Yilin Wang,* and Lei Jiang**

Vast wastage of pesticides has caused significant environmental pollution and economic loss, which occurs in any step during the entire process of pesticide application. However, the existing strategies for controlling pesticide losses are step specific. Here, a comprehensive strategy to substantively improve pesticide efficiency on the basis of precise designs from beginning to end is developed. A water-based coacervate with synthesized imine-based dynamic covalent trimeric surfactants to synergistically control encapsulation, deposition, retention, and release of pesticides on water-repellent plants is constructed. The coacervate consists of nanosized networks and abundant tightly bonded water, leading to effective encapsulation of hydrophilic/hydrophobic pesticides. Meanwhile, the network-like microstructure entangles with the micro/nanostructures of superhydrophobic surface, ensuring complete deposition on superhydrophobic plant surface after high-speed impact and inhibition of wind/rainwater erosion. Moreover, the CO_2-induced degradative surfactant coacervate determines the precise pesticide release. The dynamic coacervate as an innovative pesticide formula provides a prospective way for pesticide application, and is expected to promote productive and sustainable agriculture.

1. Introduction

Pesticides are indispensable for modern agriculture, save 30–40% crops, and will continue to increase the overall agricultural production to meet 9.7 billion people in 2050.[1–3] Conventional pesticide formulas, mainly emulsifiable concentrate (EC) and wettable powder (WP), easily drift, runoff, and scour into the environment, and loaded active ingredients are largely decomposed and leached due to poor pesticide encapsulation.[4,5] The actual uptake of pesticides by biological targets is less than 1.0%.[6–8] To achieve insecticidal effect, pesticides have to be seriously overused and have reached 4.1 million tons per year worldwide. The lost pesticides and large amounts of organic solvents in pesticide formulas have caused a series of ecological and environmental problems and have even harmed human health.[7,9–11] Therefore, sustainable agriculture demands the elimination of organic solvents and improvement of pesticide efficiency. Desired pesticide formulas are mainly aimed at taking water as solvent and require that pesticides must be 1) well encapsulated, 2) completely deposited after spray, 3) firmly remain under wind and rain erosion, and 4) precisely released so as to reduce use amount and application frequency.[4–6,12–14]

During water-based pesticide applications, the spray process is responsible for 50% of pesticide loss.[4,8] The very short contact time of spray droplets on a water-repellent leaf surface results in unavoidable bouncing and splashing.[15–17] The contact time is defined as the time the sprayed droplets take from contacting the solid surface to bouncing off the surface, generally including a spread stage and extraction stage. The characteristic time scale of water droplets is low to several milliseconds on superhydrophobic surface. To enhance pesticide utilization efficiency, mainstream researches have therefore established sub-micrometer-scaled assemblies and capsules to maximize the specific area for inhibiting rebound,[18–20] enhancing retention,[21,22] and controlling pesticide

B. Liu, Prof. Y. Fan, H. Li, W. Zhao, S. Luo, H. Wang, B. Guan, Q. Li, J. Yue, Prof. Y. Wang
CAS Key Laboratory of Colloid
Interface and Chemical Thermodynamics
CAS Research/Education Center for Excellence in Molecular Sciences
and Beijing National Laboratory for Molecular Science
Institute of Chemistry
Chinese Academy of Sciences
Beijing 100190, P. R. China
E-mail: yxfan@iccas.ac.cn; yilinwang@iccas.ac.cn

The ORCID identification number(s) for the author(s) of this article can be found under https://doi.org/10.1002/adfm.202006606.

Prof. Z. Dong, Prof. L. Jiang
CAS Key Laboratory of Bio-inspired Materials and Interfacial Sciences
Technical Institute of Physics and Chemistry
Chinese Academy of Sciences
Beijing 100190, P. R. China
E-mail: dongzhichao@iccas.ac.cn; jianglei@iccas.ac.cn

Prof. Z. Dong, Prof. L. Jiang
University of Chinese Academy of Sciences
Beijing 100049, P. R. China

DOI: 10.1002/adfm.202006606

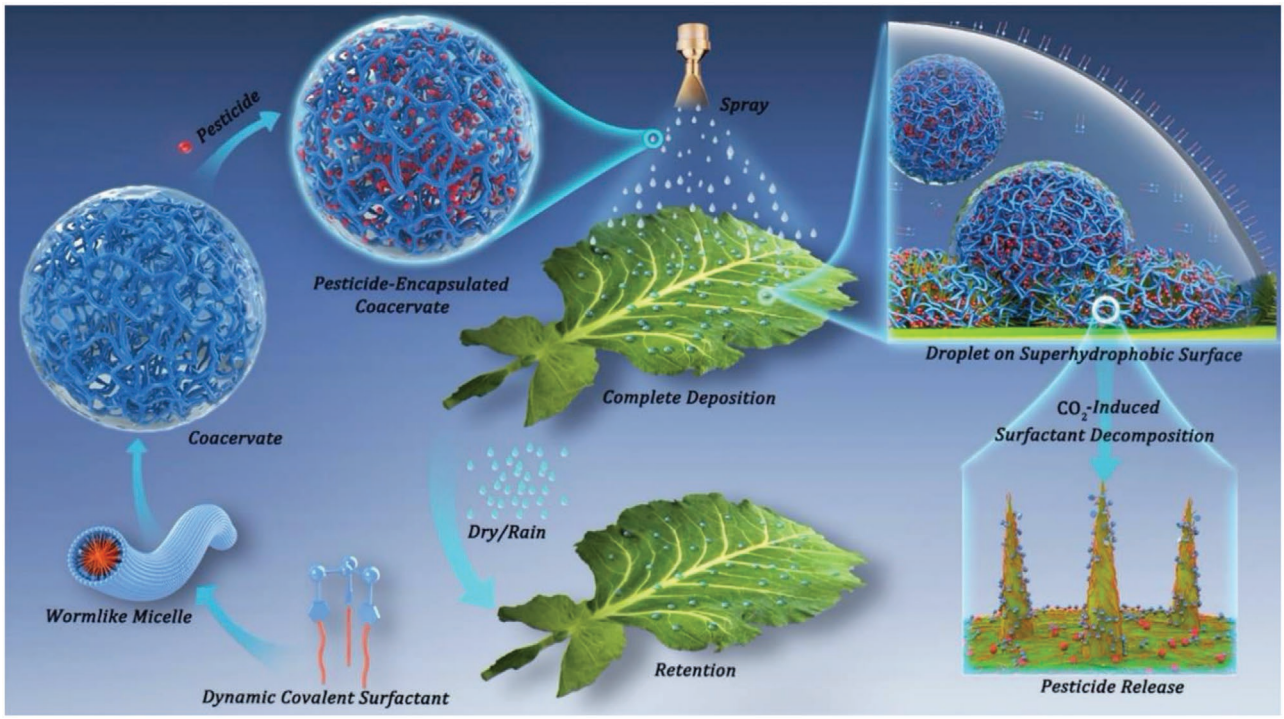

Scheme 1. Schematic of the strategy for controlling the entire journey of pesticide application on a superhydrophobic plant surface. Dynamic covalent surfactant self-assembles into coacervate, with intermediate assembly of wormlike micelle. Then, pesticide is easily and completely encapsulated by coacervate. The pesticide encapsulated coacervate fully realizes the impact deposition on super-hydrophobic leaf surface, excellent anti-rainwater erosion performance, and controlled release of pesticide, which inhibit pesticide loss covering multiple aspects and provides a new and feasible strategy for the design of pesticide formulation with comprehensive abilities.

release.[5,23] Unfortunately, the assemblies applied to inhibiting the rebound have not considered the encapsulation ability and control release. On the contrary, the capsules specially targeted for active ingredient encapsulations[24–27] are unable to enhance droplets deposition or long-term adhesion on the superhydrophobic surface due to rigid structure and low permeability.[28,29] Moreover, the capsules applied in encapsulating pesticide active ingredients still suffer from complex manufacture, poor encapsulate efficiency, incompletely release, and unavoidable organic solvents usage. As a result, existing strategies for controlling pesticide loss and environmental pollution still fail to work at two or more aspects in all the pesticide application stages.

To address these problems, herein we design and synthesize imine-based dynamic covalent surfactants, and develop a comprehensive pesticide formulation to improve the pesticide utilization efficiency from all the aspects, including encapsulation, deposition, anti-wind/rainwater erosion, and release. As **Scheme 1** depicts, the synthesized imine-based dynamic covalent trimeric surfactants show self-coacervation property on the basis of the strong aggregation ability of oligomeric surfactants. The surfactant-based coacervate does not need any organic solvents. Moreover, because of high surface activity and nanosized micelle network, the surfactant coacervate facilely encapsulates hydrophilic/hydrophobic pesticides and exhibits superior affinity to the epicuticular wax and micro/nanostructures of superhydrophobic leaf surface. The latter endows the coacervate with complete deposition on superhydrophobic surface after high-speed impact and the wind/rainwater resistance during the subsequent application stages. Due to the dynamic imine bonds in the trimeric surfactant, the coacervate can also precisely control the pesticide release with the act of CO_2. Our method provides a new and feasible strategy for the pesticide formula with comprehensive abilities.

Active ingredients of pesticides are high melting-point hydrophobic solid or hydrophilic compounds. Normally coacervate is formed by the association of amphiphilic colloidal components in water,[30] and is supposed to show functional loading and releasing capacity for both hydrophilic and hydrophobic substances,[31–34] and superior adhesive ability to a wet solid surface.[35,36] Herein, the surfactant coacervate was designed with three goals in mind: first, to synthesize an aqueous capsule with high loading efficiency and capacity to both hydrophobic and hydrophilic pesticides, second, to make the capsule with high affinity to superhydrophobic surface after high-speed impact, and third, to make the capsule with environment-controlled dissociation and release property.

2. Results and Discussion

2.1. Synthesis of Dynamic Covalent Trimeric Surfactants and Coacervate Preparation

Traditional surfactants rarely generate coacervate by themselves and often demand severe conditions. By comparison, oligomeric surfactants[37,38] with three or more amphiphilic

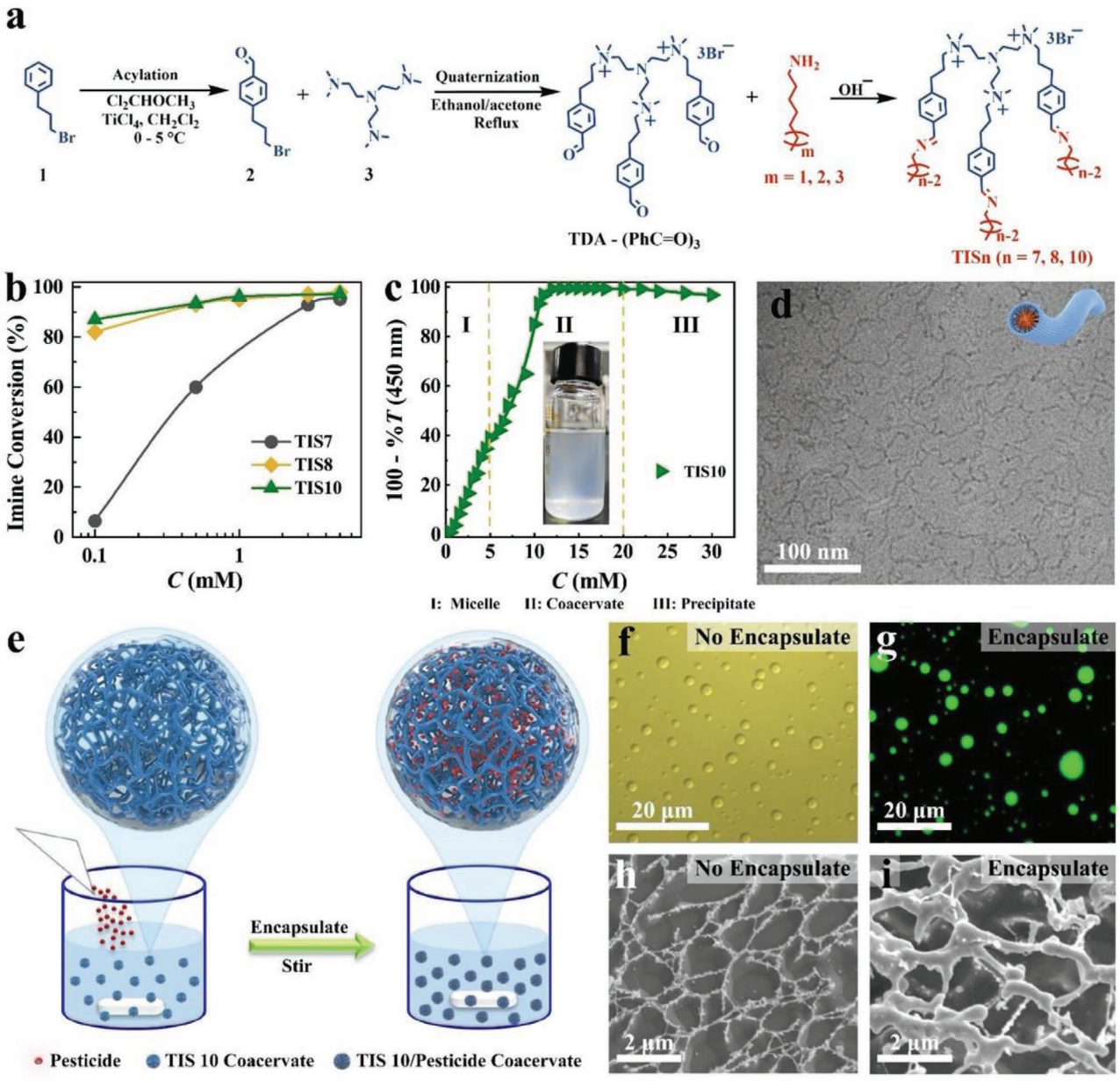

Figure 1. Surfactants characterization and pesticide coacervate preparation. a) Synthetic route of imine-based covalent trimeric surfactants with different hydrophobic chain length; b) Imine conversion rate characterized by ^{1}H NMR increases with increasing the surfactant concentration and the hydrophobic chain length for the three surfactants, in which TIS8 and TIS10 have high conversion rate even at a concentration lower than 0.1 mM in water of pH 12.5; c) Turbidity graph of TIS10 solution shows it experiences micellization, coacervation, and precipitation with increasing the concentration, and the critical coacervate concentration is 4.8 mM at pH 12.5; the inserted image is of 5.0 mM TIS10 coacervate dispersion; d) Cryo-TEM image of 2.5 mM TIS10 shows wormlike micelles; e) Schematic illustration for TIS10 coacervate solution encapsulating pesticides; f) Optical microscopy; g) CLSM images show a great number of coacervate microdroplets, and h,i) Cryo-SEM images show nanosized network structure of the coacervate of 5.0 mM TIS10 with or without the pesticide being encapsulated. All experiments are completed at 25.0 ± 0.5 °C.

moieties show much stronger self-assembling ability and more acting sites, facilitating the formation of coacervate. Meanwhile, dynamic imine bonds[39–41] may render the coacervate with environment-responsive dissociation and pesticide release. On the basis of these principles, we designed and synthesized the novel dynamic covalent trimeric surfactants through connecting three hydrophobic alkyl chains with cationic headgroups by imine bonds (**Figure 1**a). Surface inactive cationic trimeric headgroup TDA-(PhC = O)$_3$ was synthesized (Figures S1 and S2, Supporting Information) from 1-bromo-3-phenylpropane (compound 1), by acylation and quaternization with 1,1-dichlorodimethyl ether and tris[2-(dimethylamino) ethyl] amine (compound 3) under catalyzation, respectively. Then, a series of imine-based trimeric surfactants, TISn (n = 7, 8, and 10, standing for the length of hydrophobic chain), are separately obtained by mixing TDA-(PhC = O)$_3$ with heptylamine,

octylamine, and decylamine under alkaline condition (Figure S3, Supporting Information).

The surfactant TIS10 with the longest hydrophobic chains shows the highest transformation rate (Figure 1b), and the lowest critical micelle concentration (CMC, ≈1.5 μM) (Figures S4 and S5, Supporting Information). Upon increasing the surfactant concentration, the size of surfactant micelles increases (Figure S6, Supporting Information) and the solution changes from transparent to turbid (Figure 1c, Figure S7, Supporting Information). The cryogenic transmission electron microscope (Cryo-TEM) image (Figure 1d) shows that 2.5 mM TIS10 forms a number of wormlike micelles with a size of about 2–3 × 100 nm. The extremely small zeta potential (ζ) value (0.834 ± 0.062 mV) indicates the wormlike micelles tend to crosslink with each other. As expected, the further association of them takes place and coacervate is formed at a higher concentration (Figure 1c inset), which is evidenced by a lot of 1–2 μm-sized spherical microdroplets under light microscopy (5.0 mM TIS10, Figure 1f). The cryogenic scanning electron microscope (Cryo-SEM) image presents a randomly entangled network structure with nanosized fibers in coacervate droplets (Figure 1h), which is rich in both hydrophobic microdomain and hydrophilic interface. Oligomeric surfactant has shown many unique aggregation behaviors, but to the best of our knowledge, there are no known examples of oligomeric surfactant with self-coacervation property. Moreover, TIS10 displays a superior self-coacervation ability compared with the other two, of which the critical coacervate concentration is the lowest (15.8, 8.4, 4.8 mM for TIS7, TIS8, and TIS10, Figure S7, Supporting Information). Therefore, TIS10 is chosen for all the following studies.

The nanosized networks within the coacervates facilitate the uptake and concentration of both hydrophobic and hydrophilic guest molecules simultaneously. Buprofezin is a representative hydrophobic pesticide with high melting-point, and has been widely used for pest control in rice, fruit, tea, vegetables, and other crops.[42] Its solubility in water, only 9.0 mg L^{-1}, limits the use for sustainable agricultural spray. By adding buprofezin solid powder directly to the TIS10 coacervate dispersion, the buprofezin-encapsulated coacervate can be prepared (Figure 1e, Figure S8, Supporting Information). Without organic solvent, 5.0 mM TIS10 dramatically enhances the solubility of buprofezin up to 916.3 mg L^{-1}, which is one hundred times larger than pure water. The encapsulation efficiency of the pesticide is quantified by inductively coupled plasma-mass spectrometry (ICP-MS) spectroscopy in the two phases, indicating that buprofezin is almost sequestered into the coacervates as long as the loading amount is without exceeding its maximum solubility. The Cryo-SEM image reveals that the buprofezin-encapsulated coacervate maintains the nanosized network structure (Figure 1i). In addition, hydrophilic pesticides are more and more desired, but it still suffers from low encapsulate efficiency and/or release lack controlled.[4,5] Herein, Fluorescein as a model hydrophilic pesticide also can be preferentially partition into the coacervates of TIS10 (Figure 1g). Its encapsulation efficiency is estimated by the ratios of the fluorescence intensities inside and out of droplets; high by up to 93%≈98% as the loading amount, and lower than 498.4 mg L^{-1} (Figure S9, Supporting Information). In brief, pesticide-encapsulated coacervate can be easily prepared and exhibits a high encapsulation efficiency to both hydrophilic and hydrophobic pesticides.

2.2. Coacervate Droplet Deposition on Superhydrophobic Surface

Enhancing deposition of high-speed impacting water droplets on water-repellent, especially superhydrophobic surface, is extremely difficult because of only several milliseconds contact time.[16,43–45] Several new approaches have been developed to improve the deposition efficiency by forming precipitate defecting,[18] transforming surface wettability,[19] and jamming the surface micro/nano structures.[20] However, the deposition and long-term performance is still a challenge for the real water-based pesticide formula. **Figure 2** shows the high-speed drop deposition of the TIS10/pesticide coacervate (Figure 2a) on superhydrophobic cabbage leaves (Figure 2b–d, Movie S1, Supporting Information).

The cabbage leaf characterized by micro/nano hierarchical structure and strong water-proof epicuticular wax layer shows the water contact angle of 156.4 ± 3.1° (Figure 2b). All the impact droplets are controlled at the diameter of 2.0 mm and the impact velocity of 2.42 m s^{-1}. While impacting the droplets of traditional suspending concentrated buprofezin formula (SC-B) of practical application concentration (0.03%), the droplets splash and bounce on the leaf surface prominently (Figure 2e). Strikingly, no splashing, bouncing, and cracking behavior takes place for the droplets of 5.0 mM TIS10 coacervate dispersion (Figure 2f) and the coacervate with encapsulated Fluorescein (Figure 2g) and buprofezin (Figure 2h). The impact outcomes show effective and complete deposition of the droplets on the superhydrophobic leaf surface. The same impact experiments are also performed on the artificial superhydrophobic surface (Figure S10, Supporting Information) and achieve similar deposition results, in which the average diameter ratio of a final spreading liquid to the initial droplet (D_f/D_o) is up to 2.8 (Figure S11, Supporting Information). The controlled liquid deposition by the act of TIS10 is capable of significantly reducing the off-target pollution of pesticides in spraying.

Why is the trimeric surfactant capable of realizing the liquid deposition and inhibiting pesticide loss from splashing and rebounding? It is noted that the dynamic surface tension of TIS10 only slightly changes within 0–0.1 s (**Figure 3**a). The surface tension can be reduced by the TIS10 molecules diffused onto the surface. At the TIS10 concentration of 5 mM, which is much higher than its CMC (≈1.5 μM), most of the surfactant molecules in the bulk exist as micelles, and the diffusion of the surfactant molecules as monomers and in micelles affects the final situations of the surfactant molecules onto the surface. This suggests that the big molecule of TIS10 and its aggregates limits the molecular diffusion from the bulk solution to the newly created interface, and thus could not lower the surface energy of a superhydrophobic substrate. Thereby, the surface tension effect of TIS10 does not play an important role, that is, the mechanism for the present trimeric surfactant in inhibiting the splashing and retracting of droplets is different from that for other surfactants.[19,20,46]

Then we turn to check the rheological property of TIS10. While impacting the TIS10 coacervate dispersion, the initial Weber number (We) is about 390 and Reynolds number (Re) is about 6 ≈ 30, showing that the inertial force drives the expansion stage ($We > 100$). The TIS10 coacervate dispersion displays larger viscosity and shear thinning property (Figure 3b), and the loss modulus (G'') is higher than storage modulus (G') for angular frequency from 0.1 to 33.0 rad s^{-1} (Figure 3c). This suggests that the

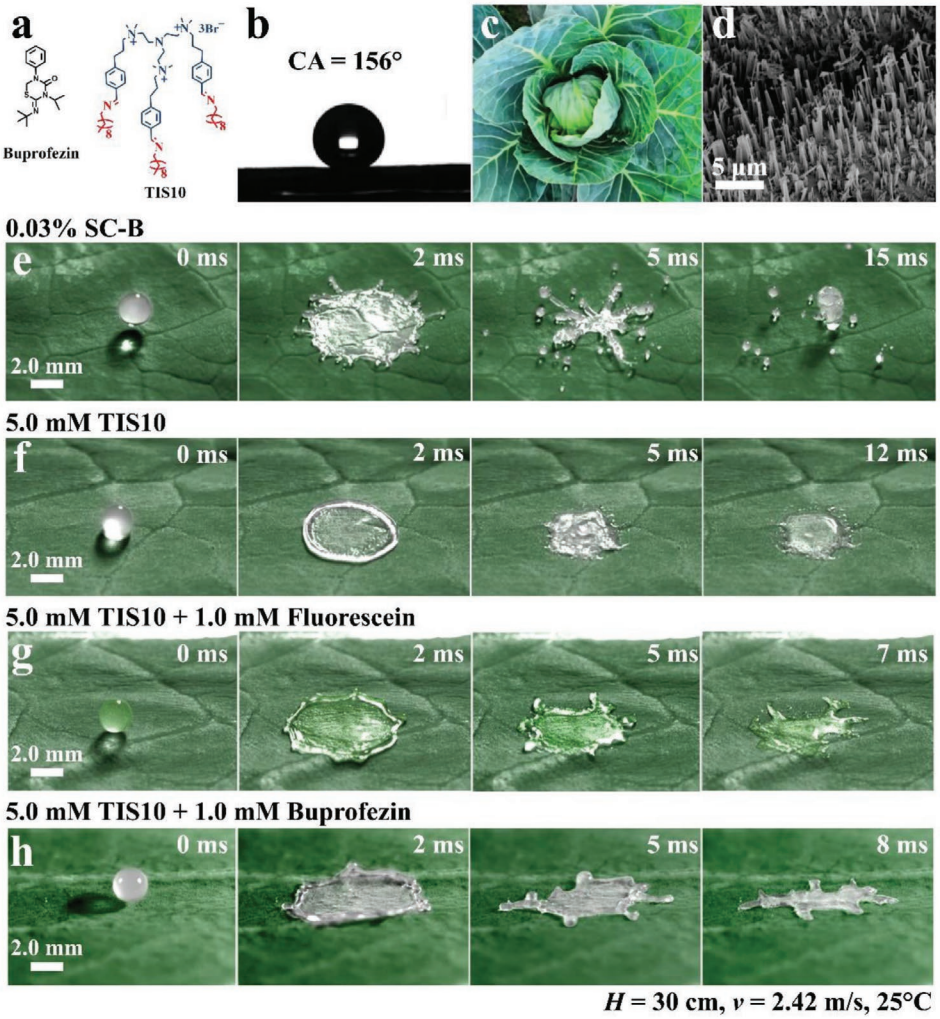

Figure 2. Drop of coacervate dispersion impacts on superhydrophobic surface as a model of the pesticide spraying process. a) Chemical structures of buprofezin and TIS10, b) water contact angle reveals the superhydrophobic property of the leaf surface, c) optical image of cabbage used, and d) SEM image of surface morphology of superhydrophobic cabbage leaf. Impact process on the cabbage leaf surface of e) traditional pesticide formula SC-B as a control shows prominent bounding and splashing. As to the coacervate dispersion of 5.0 mM TIS10 f) without encapsulation, and with encapsulated g) Fluorescein of 1.0 mM and h) buprofezin of 1.0 mM, respectively, all achieve complete deposition on the superhydrophobic cabbage leaf surface. All impact experiments with an impact velocity of 2.42 m s^{-1}.

impact kinetic energy might be dissipated during the expansion and retraction stage,[47] and thus viscous effect is possible to play a role in expanding the drop area and attenuating drop retraction. Nevertheless, we found even if the TIS10 wormlike micelle solution (4.0 mM) own a very similar rheological property to the TIS10 coacervate dispersion (Figure 3b,c), the micelle droplets rebound prominently from the surface (Figure S12, Supporting Information). Therefore, the viscosity is also not the determinative role to the complete deposition of the TIS10 coacervate on the surface.

We thus infer that the complete deposition should stem from the special dense nanosized network structure of the coacervate and the resultant certain firm pinning force between the coacervate and superhydrophobic surface. This is approved by the Cryo-SEM images (Figure 3d). The images reveal that after the droplet impact, the epicuticular nanopillars of the cabbage leaf are fully immersed by the TIS10 coacervate dispersion, clearly showing the contact line. Some of the nanopillars impale the thin liquid layer on the cabbage leaf surface, and in particular, the freeze fractured and sublimed images disclose that the coacervate spherical microdroplets firmly stick to the nanopillar of the leaf surface, demonstrating the wetting transformation from the Cassie state to the Wenzel state.

In addition, considering that the coacervate is rich in both hydrophobic microdomain and hydrophilic interface, and it is separated from the dilute equilibrium phase but still maintains liquid state, the interaction of coacervate with water is supposed to be very different from micelles. The water relaxation spectra (Figure 3e) by low-field nuclear magnetic resonance (LF-NMR) indicate that the amount of tightly bound water (corresponding to the left peaks around 1 ms) by TIS10 coacervate, no matter with or without pesticides (16.8%, 13.0%, 11.7%), is much larger than that by SC-B (3.2%) or TIS10 wormlike micelles (5.6%). The stronger ability of binding water should be beneficial for the coacervate to bind with various specific polar microregions at the superhydrophobic leaf surface and helpful for the surface wettability transition from superhydrophobic to hydrophilic.

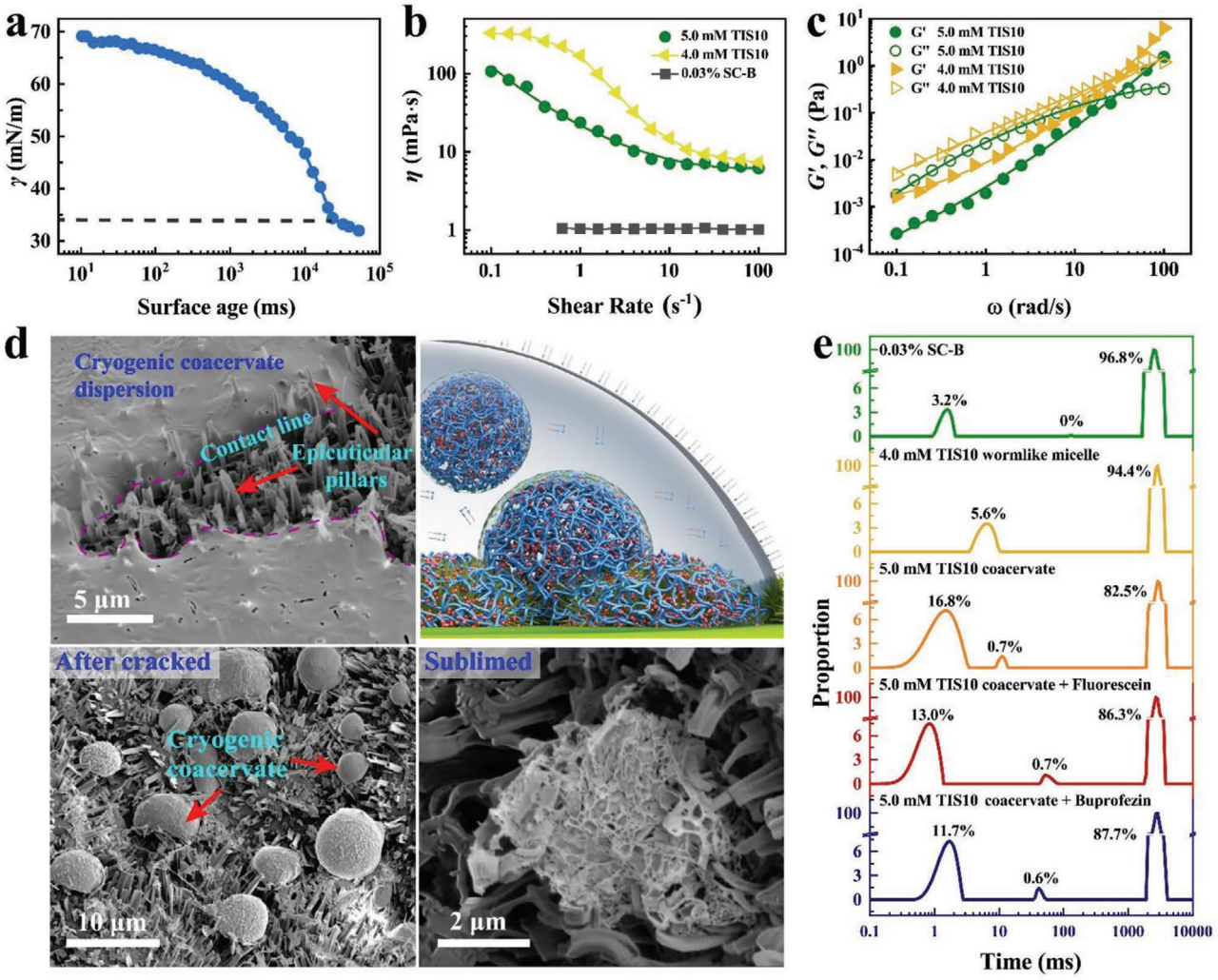

Figure 3. Mechanism of the deposition of high-speed impact coacervate drop on the superhydrophobic surface. a) Dynamic surface tension curve of TIS10 coacervate dispersion at 5.0 mM shows slow dynamic of TIS10, b) Steadily-shear rheological data of 5.0 mM TIS10 coacervate with comparison to wormlike micelle solution of 4.0 mM TIS10 and 0.03% SC-B, showing the moderate viscous and shear thinning property of TIS10 coacervate but not viscous of SC-B. c) The dynamic rheological test indicates viscous behavior (*G″*) dominate for both of 5.0 mM TIS10 coacervate dispersion and wormlike micelle solution of 4.0 mM TIS10. d) Cryo-SEM images demonstrate a coacervate droplet entangled with the micro/nano- hierarchical structure of the Cabbage leaf surface. The two images at the bottom are freeze fractured states of the upper left image. The upper right image shows its model. e) Relaxation time spectra of water for the TIS10 coacervate dispersion with and without encapsulation characterized by LF-NMR, with comparison to the TIS10 micelle solution and suspending concentrated buprofezin (SC-B). Peaks of short relaxation time in left correspond to the bound water, while peaks of long relaxation time in right correspond to the free water. All the above experiments are completed at 25.0 ± 0.5 °C.

2.3. CO_2-Induced Coacervate Dissociation and Controlled Pesticide Release

After pesticides are effectively deposited on crop surfaces, the control release of pesticides becomes a key step to ensure the long-term activity of pesticides. The longer release time means more of a tendency to keep pesticides on a leaf surface. CO_2 is ubiquitous in a natural environment and can acidify the TIS10 solution and in turn dissociate the imine groups (**Figure 4**a). With the injecting of CO_2 into the TIS10 solution, the pH declines from 12.5 to 8.4 and further down to 5.8, correspondingly, the imine groups are partially hydrolyzed and completely dissociated in the final state(Figure 4b, Figures S3 and S4, Supporting Information). As a result, the coacervate is also dissociated. On the basis of this property, more than 80% hydrophilic Fluorescein and hydrophobic pesticide buprofezin can be released in 24 and 40 h (Figure 4c), respectively. While utilizing the CO_2 in air, the same release process was completed in three months. The images captured by confocal laser scanning microscopy (Figure 4d) present the kinetic release process and the coacervate dissociation: Fluorescein is initially enriched in the coacervate microdroplets; when the pH changes to 10.5, the coacervate microdroplets are partially dissociated; further decreasing pH down to 9.5, most Fluorescein is released into the solution but some Fluorescein is still kept in the smaller coacervate microdroplets; and finally when the pH decreases to 5.8, the TIS10 coacervate microdroplets are dissociated and Fluorescein is released completely. Therefore,

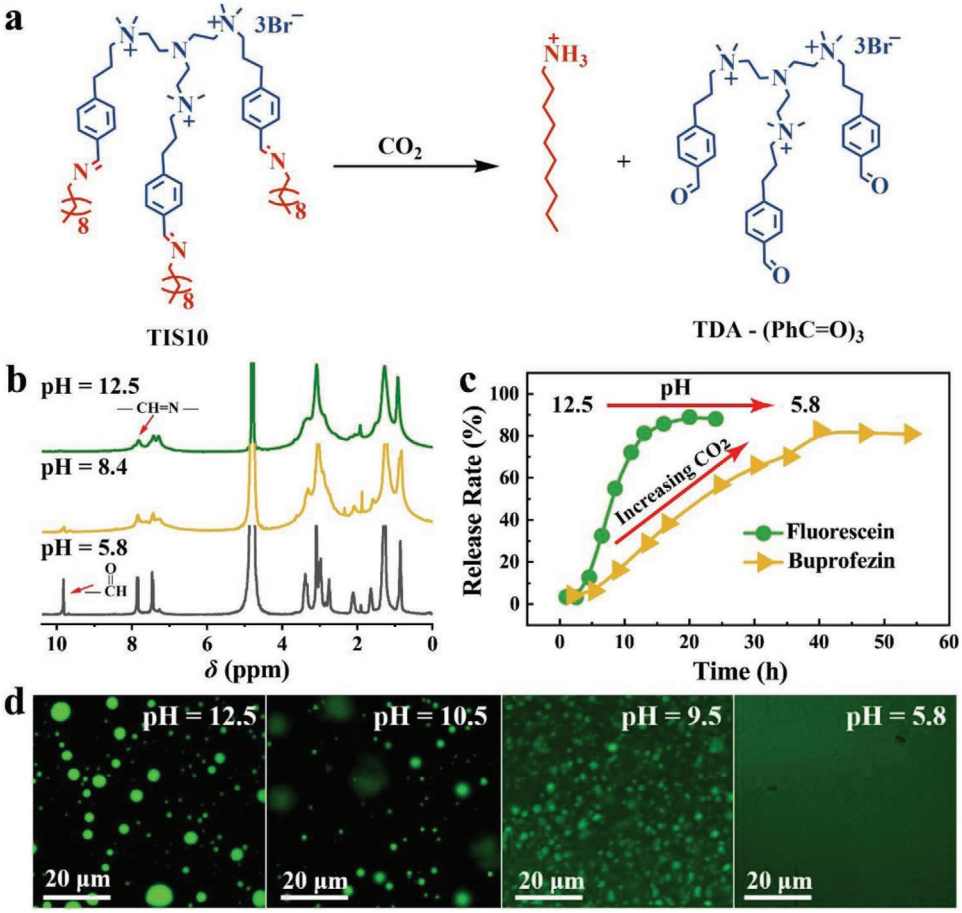

Figure 4. Characterization of surfactant dissociation and pesticide release by TIS10 coacervate. a) Schematic of TIS10 dissociation under CO_2. b) ^1H NMR spectra for TIS10 of 3.0 mM at pH 12.5, 8.4, and 5.8 respectively, demonstrating imine is gradually dissociated into aldehyde by CO_2 admission and the resultant pH declines, and when pH down to 5.8, imine is completely decomposed. c) Release profile of Fluorescein and buprofezin encapsulated by the TIS10 coacervate of 3 mL in 60 mL releasing medium with increasing CO_2 input time at a flow rate of 6 mL min^{-1}. d) CLSM images of Fluorescein-encapsulated TIS10 coacervate with the pH decrease by inputting CO_2, showing gradual coacervate dissociation and Fluorescein release. All the above experiments are completed at 25.0 ± 0.5 °C.

the precisely controlled and complete release of pesticides is achieved by controlling pH with applying CO_2. Besides in air, CO_2 can be also generated by plant respiration and water transpiration, and the nanosized micelle network microstructure of coacervate has strong hydration ability, so this CO_2-induced degradative surfactant-based coacervate should be favorable for retaining water and continuously releasing pesticides. The pesticide dose released by CO_2 at crop surface may adapt to the different growth periods of various crops, and thus be the smart doses.

2.4. Adhesion and Rainfastness

Pesticide deposited on crop leaves often loss from wind or rain under the natural environment.[4,48] The extended-release time of pesticides requires the sufficient adhesion of the coacervate on the superhydrophobic leaf surface. The network structure of the coacervate could be a robust design to overcome this problem due to its strong binding with the superhydrophobic surface.

To evaluate the wind influence, we assess the adhesive ability of the TIS10 coacervate on the cabbage leaf surface by spinning under the centrifugal force of 16.4 folds of mass, with comparison to SC-B and TIS10 micellar solution. As revealed by the time-sequence images (**Figure 5**a), all the drops tend to lean forward at the beginning, then gradually elongate, and finally throw out the front part. But the retention time of the TIS10 coacervate droplet is nearly five-times to that of SC-B and the TIS10 micelle solution (Figure 5b). We have also measured the advancing and receding contact angles of TIS10 coacervate dispersion on superhydrophobic surface. However, there is a motionlessness of the droplet when it contacts the superhydrophobic substrate and whatever the tilt angle of the substrate (Movie S2, Figure S13, Supporting Information). That is to say, the coacervate possesses the superior pinning ability on the leaf surface.

Then we tend to evaluate the rainfastness of the TIS10 coacervate droplet by testing the scour performance. Samples are naturally dried on cabbage leaf surface to imitate the real state of pesticide mostly in a natural condition. Fluorescein is washed away and almost bare in SC-B just as it contacts rainwater. In

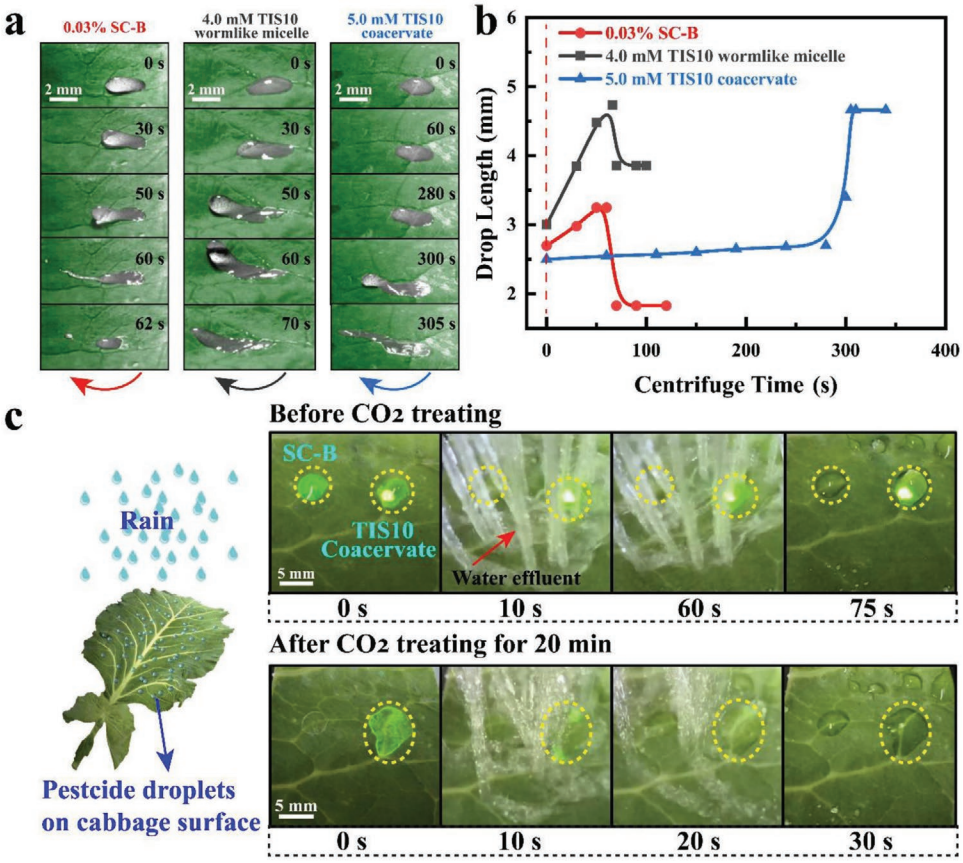

Figure 5. Adhesion ability and rainfastness characterization. a) Images of drop adhesion state on cabbage leaf surface vary with the spinning time, the arrows indicating spinning direction, the rotating speed is 500 rpm, and the initial position distance of drop sample from the center is 6.0 mm. b) Drop length of 5.0 mM TIS10 coacervate dispersion varies with centrifuge rotation time, compared with 0.03% SC-B solution and 4.0 mM TIS10 wormlike micelle solution. The coacervate droplet shows a sixfold time to the other two in resisting wind on the cabbage leaf surface. c) Rain erosion test of the TIS10 coacervate with encapsulated 0.03% buprofezin and 0.1 mM Fluorescein on cabbage leaf surface with comparison to SC-B. The yellow dash circles indicate the sample positions. The disappearance of green fluorescence in the circle of SC-B at 10 s represents that SC-B is washed away. The long-time existence of the green fluorescence indicates that the TIS10 coacervate owns superior adhesive ability on the superhydrophobic cabbage leaf surface, but it can be washed away after CO_2 treatment for a relatively long time. All the above experiments are completed at room temperature.

contrast, Fluorescein-encapsulated TIS10 coacervate remains intact and emits a strong green fluorescence under 70 s wash (Figure 5c, Movie S3, Supporting Information). This means that the coacervate has strong anti-rain ability on the superhydrophobic cabbage leaf surface, ensuring the long-term validity of the pesticides.

Even if treating the coacervate with CO_2 for 20 min makes it dissociate partly, the drop still withstands a short period of pour rain erosion, but it is thoroughly washed off after 30 s (Figure 5c, Movie S4, Supporting Information), which ensures the sustained release for the later application period of pesticides and no pesticide residue on crops finally. Moreover, owing to the very low critical micelle concentration of the trimeric surfactant and the large size of the formed coacervate, the surfactant penetration into the plant tissue can be greatly inhibited according to the principle of surfactant penetration.[49] Undoubtedly, all these greatly contribute to the safety of final crop products.

In addition, when the coacervate is naturally dried on the leaf surface, the SEM images suggest that a continuous film exists on the external surface but maintains a loosely nanosized network inside (Figure S14, Supporting Information). This structure is favorable for retaining water, continuously releasing pesticides as well as bioavailability. Therefore, the coacervate formulation can keep its entire functions under a natural condition.

3. Conclusion

Taken together, our research provides a sustainable and innovative pesticide formulation relying on dynamic oligomeric surfactant coacervate to enhance the efficiencies by controlling the entire journey of pesticide application. The nanosized network microstructure in the coacervate enriches both hydrophilic and hydrophobic domains and strongly entangles with the superhydrophobic surface, making the surfactant coacervate efficiently encapsulate hydrophilic/hydrophobic pesticides by direct mixing, inhibit drop splash and rebound from the surface after high-speed impact, and can keep long-term performances by anti-wind/rain erosion ability. Moreover, the dynamic covalent bonds in the surfactant

molecule endow the coacervate with environment-responsive dissociation and CO_2-controlled complete release. We believe that this comprehensive strategy would address the challenge from the inefficient use of pesticides, which has caused severely negative influences on biodiversity and current unsustainable agricultural practices in the face of a growing population. Furthermore, we envision that the innovative pesticide formulation would promote scientific fundamentals and technological applications in other fields, such as active substance immobilization and an intelligent biological nanodevice adhesive on both artificial and natural surfaces.

4. Experimental Section

General Information: 1-Bromo-3-phenylpropane (98%), tris[2-(dimethylamino) ethyl] amine (99%), octylamine (99%), and hydrogen bromide were purchased from Alfa Aesar. Heptyl amine (99%), decylamine (99%), Nile red (99%), sodium deuteroxide (NaOD, 99%), and deuteroxide chloride (DCl, 99%) were purchased from Acros Organics. 1,1-dichlorodimethyl ether (Cl_2CHOCH_3, >97%) was purchased from Adamas, titanium tetrachloride ($TiCl_4$, 99.9%), and buprofezin (99.5%) was purchased from Aladdin. Fluorescein was purchased from J&K Chemical. Deuteroxide was from Innochem. A sodium hydroxide standard solution was purchased from TCI. All organic solvents used in the experiments were purchased from Beijing Chemical Works. All the materials and solvents were used as commercial suppliers without further purification. Deionized water (18.2 MΩ cm) from Milli-Q equipment was used in all experiments. The cabbage leaf of 70 days age was obtained from the Institute of Vegetables and Flowers, Chinese Academy of Agricultural Sciences. The ^{1}H NMR and ^{13}C NMR of all the substances were recorded on a Bruker Avance 400 MHz spectrometer. Mass spectra were recorded on a Thermo Exactive spectrometer for ESI and Waters GCT for EI. UV–vis spectra were recorded in quartz cuvettes (light path 10 mm) with a Hitachi U-3900 spectrophotometer. Fluorescence spectra were measured on a Hitachi F-4600 spectrometer in a quartz cell with 10 mm path length. Transmission electron microscopy (TEM) was captured by JEM-2011 with accelerating voltage 120 kV.

Synthesis of TISn: *p*-(bromopropyl) benzaldehyde was synthesized (Figures S15 and S16, Supporting Information) via a literature procedure.[41] TDA-$(PhC=O)_3$ was synthesized from the quaternization reaction of *p*-(bromopropyl) benzaldehyde and tris[2-(dimethylamino) ethyl] amine with 5:1 ratio in acetone/ethanol (10:1, v/v%) under nitrogen atmosphere and reflux. After the solution was stirred and refluxed for 56 h, the solution was cooled to room temperature, added excess acetone and filtered to obtain yellow precipitates. With recrystallized by isopropanol/dichloromethane for three times and then recrystallized by acetone/ethanol for twice, TDA-$(PhC=O)_3$ was obtained as light-yellow crystal with yield of 40%. ^{1}H NMR (D_2O, 400 MHz, ppm): δ 9.84(s, 3H, CHO), 7.87 (d, 6H, CH), 7.46 (d, 6H, CH), 3.38 (m, 12H, N^+-CH_2-N, N^+-CH_2-Ar), 3.09 (s, 18H, N^+-CH_3), 3.00. ^{13}C NMR (125 MHz, D_2O): δ 195.84, 148.27, 134.16, 130.52, 129.26, 64.23, 60.48, 51.09, 46.62, 31.60, 23.44. HRMS-ESI (m/z): calculated for $C_{42}H_{63}N_4O_3Br_3$, 911.7; found 223.8 [M-3Br–]3^+/3); 376.2 [M-2Br$^-$]2^+/2); 831.7 [M-Br$^-$]$^+$).

Characterization of Surfactant and Coacervate: Surface tension was measured by DCAT21 tensiometer (DataPhysics Co., Germany). The critical micelle concentrations of surfactants were determined from the break of surface tension curves. The surfactants aggregates were measured by a DLS spectrometer (ALV/SP-125) and visualized by Cryo-TEM (JEM-2011, JEOL) at about –174 °C. Zeta potentials were determined on a Malvern Zetasizer Nano ZS. Turbidity curves of the surfactant solutions were measured at 450 nm using a Brinkman PC950 probe colorimeter. The maximum Nile Red emission wavelength (λ_{max}) at different pH was recorded by a fluorescence spectrophotometer (F-4600, Hitachi). The coacervate morphology was characterized by light microscope (IX83, OLYMPUS), confocal laser scanning microscopy (CLSM, FV1000-IX81, Olympus), and Cryo-SEM (S-4300, HITACHI) equipped with cryo-preparation chamber (EM ACE600, LEICA) at –137 °C. Steady and dynamic rheological experiments were performed on an MCR302 stress-controlled rheometer (Anton Paar OptoTec, Germany).

Pesticide Encapsulation: Pesticide coacervate was prepared by mixing hydrophobic pesticide buprofezin or hydrophilic model pesticide Fluorescein with the surfactant coacervate dispersion. Buprofezin was completely encapsulated by TIS10 coacervate below the loading capacity. The efficiency of Fluorescein encapsulated by the coacervate was tested by determining the unencapsulated Fluorescein concentration with the UV–vis absorption of the upper solution after centrifugation. The encapsulation efficiency of buprofezin is quantified by ICP-MS spectroscopy in the two phases. The encapsulation efficiency and loading capacity were separately determined as the percentage of the weight of encapsulated pesticide to the weight of the initial added pesticide, or to the weight of surfactant used.

Fabrication of Superhydrophobic Surfaces: A dip-coating method via a literature procedure[20]was employed to fabricate a superhydrophobic surface on a glass substrate. The contact angle of water was tested about 160.4 ± 2.3°. The contact angle was measured using a contact angle measurement device (DSA100, KRUSS). The CA values were obtained by measuring more than three different positions on the superhydrophobic surface.

Drop Impacting on Superhydrophobic Surface: Drop impact velocity was controlled at 2.42 m s^{-1} by free falling the droplet from a stainless-steel syringe needle with a settled height. The diameter of the liquid drop was controlled at 2.0 mm by adjusting the inner diameter of the needle. The droplet impacting dynamics on a superhydrophobic surface was captured by a high-speed camera (FASTCAM Mini UX100 Photron) at a frame rate of 2000 fps with a shutter speed 1/20000 s. The PPI of the impact test images are 1000 × 682.

CO_2-Induced Fluorescein and Buprofezin Release: The controlled-release property of Fluorescein and buprofezin encapsulated in coacervate was evaluated by dynamic dialysis method. The TIS10/Fluorescein coacervate dispersion was added into a dialysis membrane (with a molecular weight cutoff of 3500 Da), and the end-capped dialysis membrane was put into a beaker with pure water as the release medium, stirred at 150 rpm and 25 °C. At various time intervals, the solution outside the dialysis membrane was withdrawn, mixed with Na_2HPO_4 to reach pH 9.2, and the released Fluorescein concentration was measured by a UV–vis spectrophotometer to determine the kinetic profile of release (Figure S17, Supporting Information). The release procedure of buprofezin was the same as that of Fluorescein, but taking 30% ethanol-water as a release medium. The buprofezin concentration was quantified by detecting $^{32}S^{16}O$ with field inductively coupled plasma mass spectrometer (ICP-MS) by S standard addition method (Figure S18, Supporting Information). The final accumulated release data was calculated by summing up the released buprofezin or Fluorescein mass divided by the mass of feed. Micro state of coacervate during the release was visualized by CLSM (FV1000-IX81, Olympus). The pH of each sample was adjusted by CO_2 injection at different times and ensured equilibrium before imaging.

Characterization of Adhesion Ability and Rainfastness: Droplet adhesion was characterized by a spin coater to imitate wind erosion. The controlled drop volume was 8.0 µL, the initial position distance of a drop from the center was 6.0 mm, and the rotating speed was 500 rpm. The adhesion state was recorded by a high-speed camera. Rain erosion test was characterized by pouring down water to the samples from a garden watering can with a spray head at a set height from the substrate. The samples of 40 µL coacervate dispersion with 5.0 mM TIS10, 0.03% buprofezin and 0.1 mM Fluorescein, and 40 µL SC-B with 0.03% buprofezin and 0.1 mM Fluorescein were parallelly titrated to the cabbage leaf surface and naturally dried for 4.0 h. The 700 µL water sprayed onto the leaf surface within ≈100 s, and each experiment was performed six times in order to confirm the observations. The process was recorded by a video camera under violet ray.

Cryogenic Transmission Electron Microscopy (Cryo-TEM): Samples for Cryo-TEM were prepared as follows: 5 µL of each sample was loaded onto a carbon-coated holey TEM grid and blotted with a filter paper

to obtain a thin liquid film on the grid. After a few seconds, the grid was quickly plunged into a reservoir of liquid ethane (cooled by liquid nitrogen) at –165 °C. The vitrified sample was then stored in liquid nitrogen until it was transferred to a cryogenic sample holder and examined with a JEOL JEM-2011 TEM (120 kV) at about –174 °C. Digital images were recorded in the minimal electron dose mode by a Gatan multi-scan cooled charge-coupled device (CCD) camera.

Cryogenic Scanning Electron Microscopy (Cryo-SEM): a) The sample solution was "sandwiched" between two gold planchettes and then plunged into liquid nitrogen slush. After that, the samples were transferred into a cryo-preparation chamber (LEICA EM ACE600) under vacuum and sublimed by cooling to –100 °C for about 15 min. The frozen surface of the samples was coated with Pt to make it conductive under an argon environment (15 mA for 200 s). Then, the samples were transferred to the cryostage of –137 °C in the microscope (S-4300, HITACHI, Ltd, Japan). Finally, imaging was performed using a 3.0 kV landing energy and 10 µA current. b) The microstates of the interface between the deposited buprofezin/TIS10 coacervate solution and the cabbage leaf surface was characterized by a scanning electron microscope (FEI Helios NanoLab G3 UC, Thermo Scientific). The coacervate solution was dripped to the cabbage leaf from a certain height, then the leaf was cut to a suitable size and glued to the sample stage by conductive tape. The leaf with coacervate solution sample was frozen in subcooled liquid nitrogen (–210 °C) and transferred in vacuum to the cold stage of the chamber, where the cryogenic sample was fractured with a cold knife and then sublimation (–90 °C, 90 min) and sputter coating (10 mA, 60 s) with platinum were conducted. Finally, the samples were transferred to another cold stage in the scanning electron microscope and imaged. The image was recorded using the electron beam at 2 kV and 0.2 nA with 15° tilt degree and a working distance of 4 mm. The resolution of the final data was 3072 × 2048.

Low Field NMR Spin-Spin Relaxation (T_2) Measurements (LF-NMR): The LF-NMR analysis was performed at room temperature by means of a Niumag Minispec NMI20 (0.47 T, 20 MHz, China). The determination of the average water protons transverse (spin-spin) relaxation time (T_2) inside the samples was performed according to the Carr–Purcell–Meiboom–Gill (CPMG) sequence[50] {90°[-τ-180°-τ(echo)]n-TR} with a 20.52 µs wide 90° pulse, echo time $\tau = 1.5$ ms, and TR (sequences repetition rate) equal to 27 s. The T_2 relaxation curve was fitted to a multi-exponential curve with the MultiExp Inv Analysis software. All the measurements were conducted six times under the same experimental condition.

Inductively Coupled Plasma-Mass Spectrometry Analyses (ICP-MS): ICP-MS spectra were achieved using a Thermo iCAP RQ field inductively coupled plasma mass spectrometer (Thermo Fisher, Germany) with a quadrupole collision-reaction cell (CRC) analyzers. The instrumental parameters are listed in Table S1, Supporting Information. The test was under O_2 gas mode, and the width of the bandpass of the quadrupole analyzer was set to the element of interest mass width. A micro-flow total consumption nebulizer (DS-1, Cetac) without drain was tested. Samples were delivered using an ASX520 (CETAC, Omaha, NE) peristaltic pump. The reduction of the amount of organic vapor entering the plasma was obtained by a Peltier-cooled spray chamber cooled down at –2 °C. The sampler and skimmer cones covered with Pt were used due to organic injection and the necessity of adding oxygen within the plasma. Pure O_2 was added between the spray chamber and the torch for the ICP-MS/MS, a typical flow of 0.2 mL min^{-1} of pure O_2 is used.

Supporting Information

Supporting Information is available from the Wiley Online Library or from the author.

Acknowledgements

The authors acknowledge project funding provided by the National Science Foundation of China (21988102).

Conflict of Interest

The authors declare no conflict of interest.

Keywords

coacervation, deposition, dynamic covalent, superhydrophobic surfaces, sustainable agriculture

Received: August 6, 2020
Revised: September 30, 2020
Published online:

[1] N. Alexandratos, J. Bruinsma, *World Agriculture Towards 2030/2050–The 2012 Revision: ESA Working Paper No. 12-03*, Agricultural Development Economics Division Food and Agriculture Organization of the United Nations, Rome **2012** www.fao.org/economic/esa.
[2] E. C. Oerke, *J. Agric. Sci.* **2006**, *144*, 31.
[3] D. Tilman, K. G. Cassman, P. A. Matson, R. Naylor, S. Polasky, *Nature* **2002**, *418*, 671.
[4] X. Zhao, H. Cui, Y. Wang, C. Sun, B. Cui, Z. Zeng, *J. Agric. Food Chem.* **2018**, *66*, 6504.
[5] S. Kumar, M. Nehra, N. Dilbaghi, G. Marrazza, A. A. Hassan, K. H. Kim, *J. Controlled Release* **2019**, *294*, 131.
[6] M. Kah, R. S. Kookana, A. Gogos, T. D. Bucheli, *Nat. Nanotechnol.* **2018**, *13*, 677.
[7] C. Lamberth, S. Jeanmart, T. Luksch, A. Plant, *Science* **2013**, *341*, 742.
[8] W. Zhang, *Proc. Int. Acad. Ecol. Environ. Sci.* **2018**, *8*, 1.
[9] S. Atashgahi, I. Sanchez-Andrea, H. J. Heipieper, J. R. D. Meer, A. J. M. Stams, H. Smidt, *Science* **2018**, *360*, 743.
[10] C. J. Topping, A. Aldrich, P. Berny, *Science* **2020**, *367*, 360.
[11] S. P. Ketan Thorat, P. K. Vemula, *Sci. Adv.* **2018**, *4*, eaau1780.
[12] G. V. Lowry, A. Avellan, L. M. Gilbertson, *Nat. Nanotechnol.* **2019**, *14*, 517.
[13] D. H. Lewis, D. R. Cowsar, *ACS Symp. Ser.* (American Chemical Society: Washington, DC) **1977**, *53*, 1.
[14] C. Gao, Q. Huang, Q. Lan, Y. Feng, F. Tang, M. P. M. Hoi, J. Zhang, S. M. Y. Lee, R. Wang, *Nat. Commun.* **2018**, *9*, 2967.
[15] A. L. Yarin, *Annu. Rev. Fluid Mech.* **2006**, *38*, 159.
[16] J. C. Bird, R. Dhiman, H. M. Kwon, K. K. Varanasi, *Nature* **2013**, *503*, 385.
[17] K. Koch, W. Barthlott, *Philos. Trans. R. Soc., A* **2009**, *367*, 1487.
[18] M. Damak, S. R. Mahmoudi, M. N. Hyder, K. K. Varanasi, *Nat. Commun.* **2016**, *7*, 12560.
[19] M. R. Song, J. Ju, S. Q. Luo, Y. C. Han, Z. C. Dong, Y. L. Wang, Z. Gu, L. J. Zhang, R. R. Hao, L. Jiang, *Sci. Adv.* **2017**, *3*, e1602188.
[20] S. Luo, Z. Chen, Z. Dong, Y. Fan, Y. Chen, B. Liu, C. Yu, C. Li, H. Dai, H. Li, Y. Wang, L. Jiang, *Adv. Mater.* **2019**, *31*, 1904475.
[21] X. Jia, W. B. Sheng, W. Li, Y. B. Tong, Z. Y. Liu, F. Zhou, *ACS Appl. Mater. Interfaces* **2014**, *6*, 19552.
[22] M. Kah, N. Tufenkji, J. C. White, *Nat. Nanotechnol.* **2019**, *14*, 532.
[23] J. C. White, J. Gardea-Torresdey, *Nat. Nanotechnol.* **2018**, *13*, 627.
[24] S. S. Datta, A. Abbaspourrad, E. Amstad, J. Fan, S. H. Kim, M. Romanowsky, H. C. Shum, B. J. Sun, A. S. Utada, M. Windbergs, S. B. Zhou, D. A. Weitz, *Adv. Mater.* **2014**, *26*, 2205.
[25] G. Dardelle, M. Jacquemond, P. Erni, *Adv. Mater.* **2017**, *29*, 1606099.
[26] D. Kumar, J. D. Paulsen, T. P. Russell, N. Menon, *Science* **2018**, *359*, 775.
[27] E. Amstad, *Science* **2018**, *359*, 743.
[28] C. Josserand, S. T. Thoroddsen, *Annu. Rev. Fluid Mech.* **2016**, *48*, 365.
[29] C. L. Hao, Y. Zhou, X. F. Zhou, L. F. Che, B. J. Chu, Z. K. Wang, *Appl. Phys. Lett.* **2016**, *109*, 021601.
[30] W. W. Zhao, Y. L. Wang, *Adv. Colloid Interface Sci.* **2017**, *239*, 199.
[31] D. J. McClements, *Adv. Colloid Interface Sci.* **2015**, *219*, 27.

[32] Z. B. Xiao, W. L. Liu, G. Y. Zhu, R. J. Zhou, Y. W. Niu, *J. Sci. Food Agric.* **2014**, *94*, 1482.
[33] T. Y. D. Tang, C. R. C. Hak, A. J. Thompson, M. K. Kuimova, D. S. Williams, A. W. Perriman, S. Mann, *Nat. Chem.* **2014**, *6*, 527.
[34] Y. Qiao, M. Li, R. Booth, S. Mann, *Nat. Chem.* **2017**, *9*, 110.
[35] R. J. Stewart, C. S. Wang, H. Shao, *Adv. Colloid Interface Sci.* **2011**, *167*, 85.
[36] B. K. Ahn, S. Das, R. Linstadt, Y. Kaufman, N. R. Martinez-Rodriguez, R. Mirshafian, E. Kesselman, Y. Talmon, B. H. Lipshutz, J. N. Israelachvili, J. H. Waite, *Nat. Commun.* **2015**, *6*, 8663.
[37] D. Danino, Y. Talmon, H. Levy, G. Beinert, R. Zana, *Science* **1995**, *269*, 1420.
[38] Y. Fan, Y. Wang, *Langmuir* **2018**, *34*, 11220.
[39] S. J. Rowan, S. J. Cantrill, G. R. L. Cousins, J. K. M. Sanders, J. F. Stoddart, *Angew. Chem., Int. Ed.* **2002**, *41*, 898.
[40] L. Tauk, A. P. Schroder, G. Decher, N. Giuseppone, *Nat. Chem.* **2009**, *1*, 649.
[41] C. B. Minkenberg, F. Li, P. van Rijn, L. Florusse, J. Boekhoven, M. C. A. Stuart, G. J. M. Koper, R. Eelkema, J. H. van Esch, *Angew. Chem., Int. Ed.* **2011**, *50*, 3421.
[42] J. C. Palumbo, A. R. Horowitz, N. Prabhaker, *Crop Prot.* **2001**, *20*, 739.
[43] L. V. Vance Bergeron, *Nature* **2000**, *405*, 772.
[44] Y. Liu, G. Whyman, E. Bormashenko, C. Hao, Z. Wang, *Appl. Phys. Lett.* **2015**, *107*, 051604.
[45] J. Su, I. Legchenkova, C. Liu, C. Lu, G. Ma, E. Bormashenko, Y. Liu, *Langmuir* **2020**, *36*, 534.
[46] X. G. Zhang, O. A. Basaran, *J. Colloid Interface Sci.* **1997**, *187*, 166.
[47] D. Bartolo, A. Boudaoud, G. Narcy, D. Bonn, *Phys. Rev. Lett.* **2007**, *99*, 174502.
[48] E. Stokstad, *Science* **2019**, *364*, 318.
[49] Y. Chen, F. Qiao, Y. Fan, Y. Han, Y. Wang, *Langmuir* **2017**, *33*, 2760.
[50] S. Meiboom, D. Gill, *Rev. Sci. Instrum.* **1958**, *29*, 688.